I.G. ORLETS'KYI, M.I. ILASHCHUK, E.V. MAISTRUK, H.P. PARKHOMENKO,
P.D. MARYANCHUK

Yu. Fed'kovich National University of Chernivtsi
(2, Kotsyubyns'kogo Str., Chernivtsi 58012, Ukraine; e-mail: i.orletskyi@chnu.edu.ua)

ELECTRICAL PROPERTIES AND ENERGY PARAMETERS OF PHOTOSENSITIVE n-Mn$_2$O$_3$/n-CdZnTe HETEROSTRUCTURES

Conditions for the fabrication of isotype photodiode n-Mn$_2$O$_3$n-CdZnTe heterostructures by the spray pyrolysis of thin α-Mn$_2$O$_3$ bixbite films on n-CdZnTe crystalline substrates have been studied. The temperature dependences of the current-voltage (I-V) characteristics were used to analyze the mechanisms of electron tunneling through the energy barrier of the heterojunction in the forward and reverse current regimes. The role of energy states at the n-Mn$_2$O$_3$/n-CdZnTe interface in the formation of the barrier parameters was clarified. Based on the capacitance-voltage (C-V) characteristics, the dynamics of changes in the capacitive parameters of the Mn$_2$O$_3$ thin film and the n-CdZnTe inversion layer and the relation between them were established. A model for the energy diagram of the n-Mn$_2$O$_3$/n-CdZnTe heterojunction was presented. The photoelectric properties of the examined heterostructure were analyzed.

K e y w o r d s: thin film, spray pyrolysis, heterostructure, energy diagram, photodiode.

1. Introduction

Manganese oxide Mn$_2$O$_3$ is known to exist in the following crystalline modifications: the cubic bixbite (α-Mn$_2$O$_3$), orthorhombic (β-Mn$_2$O$_3$), perovskite (ζ-Mn$_2$O$_3$), tetragonal (γ-Mn$_2$O$_3$), and corundum (ε-Mn$_2$O$_3$) phases [1]. Under environmental conditions, the cubic bixbite phase α-Mn$_2$O$_3$ is the most stable. It preserves its properties in wide intervals of the temperature (up to about 1200 K) and the pressure (up to about 27 GPa) [1]. The α-Mn$_2$O$_3$ compound is a widespread, non-toxic, and low-cost material. It attracts attention by its wide scope of applications in the power industry and ecology, e.g., in chemical analytics, magnetic devices, and devices for energy conversion and storage [2]. The semiconductor properties of thin films of manganese oxides are used while creating photocatalysts on the basis of 2D-2D heterojunctions with g-C$_3$N$_4$ [3] and CuO$_x$ [4] compounds, heterostructured Fe$_2$O$_3$/Mn$_2$O$_3$ electrodes for lithium energy sources [5], and gas sensors [6].

Thin α-Mn$_2$O$_3$ films are characterized by the bandgap width $E_g \approx 2.01 \div 2.4$ eV [7, 8], They are promising for the fabrication of the front layer of heterojunctions with semiconductors, which possess a high light absorption coefficient. Such a design of photodetectors is optimal for the efficient conversion of radiation energy into an electrical signal [9].

For the manufacture of thin α-Mn$_2$O$_3$ films, the spray pyrolysis [8,10] and hydrothermal [11] methods, the method of solid-state reactions in MnO$_2$ at its heat treatment [12], electrodeposition [13], and the sol-gel method [14] are applied. The advantages of the spray pyrolysis method among the others include a simple equipment and the convenient correction of the α-Mn$_2$O$_3$ film deposition mode to obtain the desired physical properties.

When depositing oxide films on substrates made of CdTe [15, 16] and solid $Cd_{1-x}Zn_x$Te solutions [17, 18], high-quality diode structures are created. This circumstance initiated us to perform an experiment aimed at the fabrication of a heterostructure based on the n-Mn_2O_3/n-CdZnTe heterojunction and the study of its electrical and photoelectric properties. Solid $Cd_{1-x}Zn_x$Te solutions with $x \leq 0.1$ are characterized by the better mechanical strength and structural perfection as compared with CdTe [19, 20]. That is why they were selected as substrates for growing α-Mn_2O_3 films. The choice of the spray pyrolysis method for the fabrication of thin α-Mn_2O_3 films was associated with its low cost and with the successful results obtained while manufacturing α-Fe_2O_3 films [15].

2. Experimental Part

For the fabrication of researched heterostructures, substrates about 1 mm in thickness split from $Cd_{1-x}Zn_x$Te ($x \leq 0.1$) crystals with the electron-type electrical conductivity, which were grown using the vertical Bridgman method, were applied. At the temperature $T = 295$ K, the substrates had the electrical conductivity $\sigma = 1.4$ $\Omega^{-1}\,cm^{-1}$ and were characterized by the free charge carrier concentration $n = 8.75 \times 10^{15}$ cm^{-3} and the electron Hall mobility $\mu_H = 1000$ cm^2 V^{-1} s^{-1}.

Isotype n-Mn_2O_3/n-CdZnTe heterostructures were fabricated by growing n-Mn_2O_3 films to the thickness $w \approx 0.5$ μm on the surface of the n-CdZnTe substrates making use of the spray pyrolysis method. The temperature of the substrates in the course of pyrolysis was maintained at the level $T_S = 350$ °C. The spray pyrolysis was performed under the atmospheric pressure. The 0.1 M solution of $MnCl_2 \cdot 4H_2O$ salt in double-distilled water was used to create an aerosol cloud over the substrates. As a result of the salt pyrolysis at the interaction with the atmospheric oxygen, there appeared a film of the binary semiconductor compound α-Mn_2O_3 (bixbite) characterized by the n-type conductivity, the resistivity $\rho \approx 10^7$ Ω cm at room temperature, and the band gap $E_g \approx 2.12$ eV. The n-Mn_2O_3 films have a high resistivity, the low coefficient of electron diffusion $D_n = 5 \times 10^{-3}$ cm^2/s [21], and the charge carrier concentration $n = 1.1 \times 10^{12}$ cm^{-3}.

Light transmission through the n-Mn_2O_3 films in the visible spectral interval was studied on a spec-
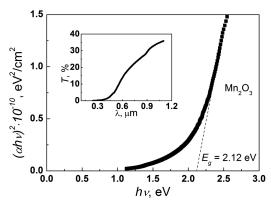

Fig. 1. Spectral dependences of the light transmission (the inset) and absorption coefficients for α-Mn_2O_3 films fabricated using the spray pyrolysis method

tral installation SF-2000. The thickness of α-Mn_2O_3 films was determined from the shift of the interference lines at the film-substrate step with the help of a Linnik microinterferometer MII-4. Ohmic contacts to the low-impedance n-CdZnTe crystals were prepared by soldering indium. Contacts to the n-Mn_2O_3 film were made using a silver-based conductive paste.

Dark and light current-voltage (I-V) characteristics of the n-Mn_2O_3/n-CdZnTe heterostructures were measured on a hardware-software Arduino complex using an Agilent 34410A digital multimeter and a Siglent SPD3303X programmable power source. The measuring complex was controlled, and the research results were preliminarily processed with the help of a computer in the LabView environment and making use of the software created by the authors. The capacitance-voltage (C-V) characteristics of the heterostructures were studied using an LCR-meter BR2876.

3. Results and Their Discussion

The α-Mn_2O_3 films with the thickness $w = 0.5$ μm which were fabricated using the method of spray pyrolysis on sodium-calcium glass substrates were characterized by the light transmittance $T = 10 \div 35\%$ in the wavelength interval $\lambda = 0.6 \div 1$ μm (see the inset in Fig. 1).

The absorption coefficient α was calculated on the basis of the value obtained for the reflection coefficient $R \approx 10\%$ [22] and using the formula [23]

$$\alpha = \frac{1}{w} \ln \left[\frac{(1-R)^2}{2T} + \sqrt{\frac{(1-R)^4}{2T^2} + R^2} \right]. \qquad (1)$$
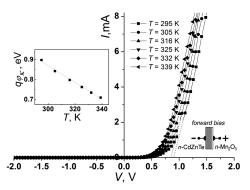
Fig. 2. *I-V* characteristics of the isotype n-Mn$_2$O$_3$/n-CdZnTe structure in the temperature interval from $T = 295$ K to $T = 339$ K and (inset) the temperature dependence of the contact potential difference $q\varphi_k$ $[d(q\varphi_k)/dT = -4.2 \times 10^{-3}$ eV/K]

On the basis of the spectral dependence $\alpha(h\nu)$, the optical width of the band gap E_g in the Mn$_2$O$_3$ films was determined in the framework of the Tauc/Davis–Mott model,

$$\alpha = \frac{B^2(h\nu - E_g)^n}{h\nu}, \qquad (2)$$

where B is a constant, and the value of the constant n is associated with the optical transition type. In particular, for allowed direct interband transitions, $n = 1/2$.

The extrapolation of the rectilinear section in the dependence $(\alpha h\nu)^2$ versus $h\nu$ toward the zero value of the absorption coefficient made it possible to obtain the optical width of the band gap, $E_g = 2.12$ eV (see Fig. 1). This value agrees well with the E_g-values given for thin Mn$_2$O$_3$ films in the literature: 2.02 eV [7] and 2.2–2.4 eV [8].

The study of *I-V* characteristics in the temperature interval $T = 295 \div 339$ K (Fig. 2) allowed us to reveal the diode properties of the isotype n-Mn$_2$O$_3$/n-CdZnTe heterojunctions. The current rectification coefficient at $T = 295$ K was about 8.75×10^3 at $|V| = 1.5$ V. The forward bias across the heterostructure, at which a drastic current growth is observed, corresponds to the voltage polarity with the negative potential applied to n-CdZnTe. The reverse biases (a negative potential at the n-Mn$_2$O$_3$ film) are characterized by insignificant current values $I_r < 3$ μA within the whole interval of examined voltages.

By extrapolating the rectilinear sections of the *I-V* characteristics registered in the forward-bias regime to the voltage axis, we estimated the height $q\varphi_k$ of the potential barrier at the n-Mn$_2$O$_3$/n-CdZnTe het-

erostructure. It was found that the quantity $q\varphi_k$ decreases linearly from 0.9 eV to 0.7 eV, when the temperature changes from $T \approx 295$ K to $T = 339$ K (see the inset in Fig. 2). The temperature coefficient $d(q\varphi_k)/dT = -4.2 \times 10^{-3}$ eV/K is within the interval typical of the CdZnTe-based heterostructures. The absolute value of this coefficient for the n-Mn$_2$O$_3$/n-CdZnTe heterostructure is an order of magnitude lower than the temperature coefficient of the band gap in the base n-CdZnTe semiconductor, $dE_g/dT = -4.01 \times 10^{-4}$ eV/K. This difference arises owing to an increase in the effective density of states N_C and N_V in the allowed energy bands, as well as in the concentration of intrinsic charge carriers, as the temperature grows [26].

To analyze the electrical properties of the n-Mn$_2$O$_3$/n-CdZnTe heterostructure, the energy diagram of a real heterojunction was used, where the influence of energy states at the n-Mn$_2$O$_3$/n-CdZnTe interface was taken into account (Fig. 3, b). When constructing the energy profile in a real n-Mn$_2$O$_3$/n-CdZnTe heterojunction, which agrees well with experimental data, a number of differences were found from the energy diagram that is based on the Anderson model and does not consider the influence of surface states and a possibility for the semiconductor energy parameters (the electron affinity χ) to change at the surface (Fig. 3, a).

Thus, when constructing the required energy diagram, we assumed that, at a low Zn concentration, the electron affinity $\chi(\mathrm{Cd}_{1-x}\mathrm{Zn}_x\mathrm{Te}) \approx \chi(\mathrm{CdTe}) = 4.28$ eV [27, 28]. The band gap in the solid solution was taken to equal $E_g(\mathrm{Cd}_{1-x}\mathrm{Zn}_x\mathrm{Te}) = 1.53$ eV [29, 30]. The electron affinity value $\chi(\mathrm{Mn}_2\mathrm{O}_3) = 4.45$ eV [10] was used, which was determined using the Kelvin probe method for Mn$_2$O$_3$ films fabricated with the help of the spray pyrolysis method. The value $E_g(\mathrm{Mn}_2\mathrm{O}_3) = 2.12$ eV was calculated from the results obtained for the optical absorption in the films (Fig. 1). The positions of the Fermi level E_F in the forbidden band gap with respect to the bottom of the conduction band in n-Mn$_2$O$_3$ ($\delta_1 = E_C - E_F \approx 0.41$ eV) and n-CdZnTe ($\delta_2 = 0.1$ eV) were determined according to the expression for the concentration of equilibrium charge carriers in nondegenerate semiconductors [31],

$$E_C - E_F = \delta = kT\ln\left[2\left(\frac{2\pi m_n kT}{h^2}\right)^{3/2}\frac{1}{n}\right], \qquad (3)$$
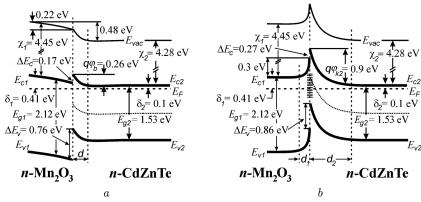
Fig. 3. Energy diagrams of the $n\text{-Mn}_2\text{O}_3/n\text{-CdZnTe}$ heterostructure at $T = 295$ K: on the basis of Anderson model (*a*) and for a real heterojunction with regard for the influence of energy states in the forbidden gap at the semiconductor interface (*b*)

where m_n is the effective electron mass in CdZnTe ($m_n = 0.096m_0$ [28]) or manganese oxide ($m_n = 0.48m_0$ [32]).

When determining the charge carrier concentration $n = 1.1 \times 10^{12}$ cm^{-3} in thin $n\text{-Mn}_2\text{O}_3$ films from the experimental resistivity value $\rho \approx 10^7$ Ω cm [according to the formula $n = (q\rho\mu_n)^{-1}$], the data on the electron diffusion coefficient $D_n = 5 \times 10^{-3}$ cm^2/s [21] were used ($\mu_n = D_n/kT$, where k is the Boltzmann constant).

According to the electron work function values for the analyzed semiconductors, $A(n\text{-CdZnTe}) = 4.38$ eV and $A(n\text{-CdZnTe}) = 4.38$ eV, the formation of an isotype $n\text{-Mn}_2\text{O}_3/n\text{-CdZnTe}$ heterojunction should enrich the $n\text{-Mn}_2\text{O}_3$ film in the majority charge carriers and diminish its resistance (Fig. 3, *a*). The distribution of the contact potential difference between the manganese oxide film, $\varphi(n\text{-Mn}_2\text{O}_3)$, and the base CdZnTe material, φ_b, is written in the form [33]

$$\varphi_b = \frac{\varepsilon_{S1}N_{D1}}{\varepsilon_{S2}N_{D2}}\left[\frac{kT}{q}\left[\exp\left(\frac{\varphi_{\text{Mn}_2\text{O}_3}}{kT}\right) - 1\right] - \varphi_{\text{Mn}_2\text{O}_3}\right], \quad (4)$$

where ε_{S1} and ε_{S2} are the relative dielectric constants of the contacting semiconductors, whereas N_{D1} and N_{D2} are the donor concentrations in $n\text{-Mn}_2\text{O}_3$ and $n\text{-CdZnTe}$, respectively. The calculated values $q\varphi(n\text{-Mn}_2\text{O}_3) = 0.17$ eV and $q\varphi_b = 0.26$ eV correspond to the E_C and E_V band bendings in the energy diagram depicted in Fig. 3, *a*.

The thickness of the electron-enriched region in $n\text{-Mn}_2\text{O}_3$, which can be estimated using the expression

for the Debye screening length [24]

$$L_D = \sqrt{\frac{kT\varepsilon_0\varepsilon_{S1}}{N_{D1}q^2}}, \quad (5)$$

equals $L_D \approx 3$ μm for $N_{D1} = 1.1 \times 10^{12}$ cm^{-3} and $\varepsilon_{S1} = 9.5$ [34]. This means that, on the basis of such speculations, an $n\text{-Mn}_2\text{O}_3$ film with the thickness $w = 0.5$ μm in the $n\text{-Mn}_2\text{O}_3/n\text{-CdZnTe}$ heterostructure is completely electron-enriched and must have a low electrical resistance. As a result, all external voltage applied across the heterojunction drops in the depletion $n\text{-CdZnTe}$ region, and the electrical properties are determined by the energy barrier with the height $q\varphi_b = 0.26$ eV. This conclusion contradicts the experimental value of the contact potential difference $\varphi_k \approx 0.9$ V (at $T = 295$ K), which was estimated from the *I-V* characteristics.

Making allowance for the negative charge of energy states in the forbidden gap at the interface between $n\text{-Mn}_2\text{O}_3$ and $n\text{-CdZnTe}$ enabled us to reconcile the experimental data with the energy parameters of the real heterojunction. The electric field created by the negative charge of the states brings about an additional energy band bending (to that obtained in the Anderson model) toward higher energies near the interface between the materials (Fig. 3, *b*). A satisfactory agreement with the experiment is obtained in the case where the energy of electrons at the heterojunction interface is increased by 0.47 eV owing to the action of the negative charge of the states. In this case, the height of the barrier on the $n\text{-CdZnTe}$ side is equal to the experimental value $\varphi_{k2} \approx 0.9$ eV, whereas the
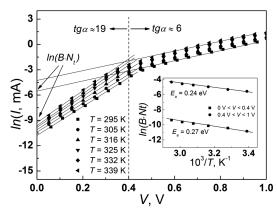
Fig. 4. Dependences of $\ln I$ on V at forward biases applied across the n-Mn_2O_3/n-CdZnTe heterostructure for various temperatures. The procedure of determining the activation energy of tunnel currents E_a is illustrated in the inset

electron depletion region with the thickness d_1, which corresponds to the barrier height $\varphi_{k1} \approx 0.3$ eV, appears on the n-Mn_2O_3 side.

When constructing the energy diagram for the n-Mn_2O_3/n-CdZnTe heterostructure, the influence of the silver contact to the n-Mn_2O_3 film on the electrical properties of the heterostructure was taken into account. Despite the high resistance of the n-Mn_2O_3 films fabricated through the spray pyrolysis, the application of silver contacts (the electron work function $A(Ag) = 4.1$ eV) leads to the enrichment of the Mn_2O_3 film [$A(Mn_2O_3) = 4.86$ eV] with electrons and reduces its resistance. Similar phenomena are observed in the ZnO:Al/CdS/CdZnTe heterostructures at the enrichment of high-impedance films of their CdS buffer layer with electrons from the transparent conductive oxide (TCO). Owing to the enrichment with the majority charge carriers, the barrier on the n-Mn_2O_3 side of the n-Mn_2O_3/n-CdZnTe heterostructure has a thickness d_1 that is much smaller than the film thickness. The thickness d_2 of the electron depletion region on the n-CdZnTe side was calculated using the formula

$$d_2 = \sqrt{\frac{2\varepsilon_0\varepsilon_{S2}\varphi_{k2}}{qN_{D2}}}, \qquad (6)$$

and the electron concentration value $n = N_D = 8.75 \times 10^{15}$ cm^{-3} so that $d_2 \approx 0.35$ μm.

In order to clarify the mechanisms of the forward current flow through the energy barrier in the n-Mn_2O_3/n-CdZnTe heterostructure, the correspon-

ding I-V characteristics plotted in the $\ln I$ versus V coordinates were used (Fig. 4). The relevant dependences are rectilinear with a temperature-independent slope angle. This is typical of the tunneling mechanism of the current flow described by the exponential dependence $I \sim \exp(\alpha V)$. In the expanded form, this dependence looks like [36]

$$I = BN_t \exp\left(-4(2m^*)^{1/2}q^{1/2}(\varphi_k - V)/3\hbar H\right), \quad (7)$$

where B is a constant, N_t the concentration of states onto which the tunneling occurs, m^* the effective electron mass (in our case, in the conduction band of Mn_2O_3), $\varphi_k = \varphi_{k2}$ is the height of the barrier through which the electrons tunnel, and $H = d_2$ is the barrier thickness (when electrons tunnel through the barrier from the conduction band in n-CdZnTe to the conduction band in n-Mn_2O_3, this parameter is determined by expression (6)).
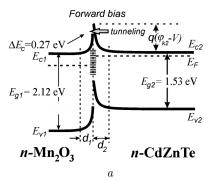
The plot of the $\ln I$-V dependence (Fig. 4) contains sections with different slopes: $\tan\alpha \approx 19$ at the voltages $3kT/q < V < 0.4$ V and $\tan\alpha \approx 6$ at 0.4 V $< V < 1$ V. Taking Eqs. (6) and (7) into account, the slope angle of the $\ln I$-V dependences is determined by the expression

$$\tan\alpha = \frac{4}{3\hbar}(m^*)^{1/2}q\left(\frac{N_{D2}}{\varepsilon_0\varepsilon_{S2}\varphi_{k2}}\right)^{1/2}. \qquad (8)$$

The decrease of the slope angle at forward voltages of about 0.4 V is associated with a reduction in the concentration N_{D2} of the electrically active impurity in the contact region on the n-CdZnTe side. For the efficient pyrolysis of the $MnCl_2$ salt and the formation of a Mn_2O_3 film on the n-CdZnTe surface, the substrate was heated to 350 °C. Under such a thermal action, some of the cadmium atoms evaporated from the near-surface region of n-CdZnTe. Cadmium vacancies are acceptors that demonstrate a compensatory effect in n-CdZnTe, when the electron concentration decreases. According to Eq. (8), the ratio

$$\frac{\tan\alpha(3kT < V < 0.4 \text{ V})}{\tan\alpha(0.4 \text{ V} < V < 1 \text{ V})} = \left(\frac{N_{D2}}{N_{D2}^0}\right)^{1/2} \qquad (9)$$

allows the contact concentration N_{D2}^0 on the n-CdZnTe side to be estimated. At the forward voltage $V \approx 0.4$ V, the electron depletion region in n-CdZnTe gets narrower (the parameter d_2 diminishes),
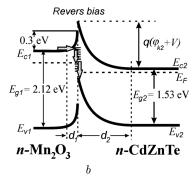
Fig. 5. Mechanisms of charge carrier tunneling through the n-Mn$_2$O$_3$/n-CdZnTe heterostructure under forward (a) and reverse biases (b)

and the concentration of the electrically active impurity decreases by an order of magnitude: from $N_{D2} = 8.75 \times 10^{15}$ cm^{-3} to $N_{D2}^0 \approx 8.8 \times 10^{15}$ cm^{-3}.

The occupation of electronic states in the conduction band of Mn$_2$O$_3$ is determined by the Fermi–Dirac distribution function, and the quantity BN_t depends exponentially on the temperature (see the inset in Fig. 4). The tangent of the slope angle in the dependences $\ln(BN_t)$ versus $10^3/T$ determines the tunneling activation energy E_a with respect to the peak of the energy barrier with the height φ_{k2} (Fig. 3, b). Within the interval of forward voltages $3kT/q < V < 0.4$ V, the activation energy $E_a = 0.27$ eV and corresponds to the tunneling of electrons through the barrier with the participation of states located in the conduction band by 0.27 eV below the peak (Fig. 5, a). At $V \approx 0.4$ V, the barrier height decreases because of a reduction in the concentration N_{D2} of the electrically active impurity in the contact region of the heterojunction. This scenario agrees well with a reduction of the tunneling activation energy to $E_a = 0.24$ eV at the voltages 0.4 V $< V < 1$ V.

The temperature-independent slope of the $\ln I$-V dependences at the reverse biases across the n-Mn$_2$O$_3$/n-CdZnTe heterostructure points to the tunneling mechanism of the reverse current formation. Within the voltage interval -0.3 V $< V < 0$ V, electrons tunnel from the states located near the bottom of the conduction band in Mn$_2$O$_3$ through a barrier with a height of about 0.3 eV (Fig. 5, b). Since the barrier is rather high, it is most probable that the tunneling is a multistage process with the participation of the states in both the n-Mn$_2$O$_3$ and n-CdZnTe band gaps at the heterojunction interface and the fur-
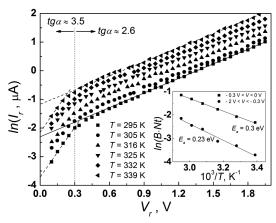

Fig. 6. Dependences of $\ln I_r$ on V at reverse voltages across the n-Mn$_2$O$_3$/n-CdZnTe heterostructure for various temperatures. The procedure of determining the activation energy of tunnel currents E_a is illustrated in the inset

ther recombination with holes in the n-CdZ inverse region. This mechanism agrees well with the activation energy of the tunnel current in the voltage interval -0.3 V $< V < 0$ V, namely, $E_a = 0.3$ eV, which was determined from the experimental dependence $\ln(BN_t)$ versus $10^3/T$ (see the inset in Fig. 6).

At the reverse biases within the voltage interval -2 V $< V < -0.3$ V across the n-Mn$_2$O$_3$/n-CdZnTe heterostructure, the activation energy of the reverse tunnel current decreases to the value $E_a = 0.23$ eV, which corresponds to a lower height of the energy barrier through which the tunneling takes place. The energy barrier with a height of 0.3 eV (at $V = 0$ V) on the n-Mn$_2$O$_3$ side is created by a negative charge of the states at the n-Mn$_2$O$_3$/n-CdZnTe interface. A reverse bias of about 0.3 V leads to the electron deoccupation of the states (the Fermi level at the hetero-

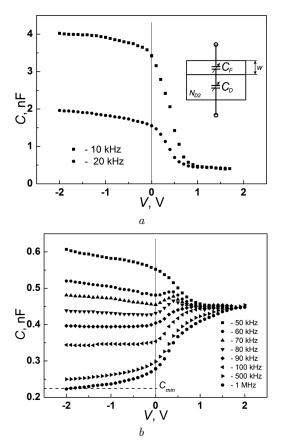**Fig. 7.** C-V characteristics of the n-Mn$_2$O$_3$/n-CdZnTe heterostructure in the frequency interval of a measurement signal 10 kHz $< f <$ 20 kHz (a) and 50 kHz $< f <$ 1000 kHz (b)

junction interface is located lower). In so doing, the negative charge of the states at the heterojunction decreases, and, as a result, the height of the tunneling barrier on the Mn$_2$O$_3$ side diminishes from 0.3 eV to 0.23 eV. The lower barrier height corresponds to the weaker electric field strength in the barrier. The rectilinear sections in the voltage interval -2 V $< V < -0.3$ V in the ln I-V dependences for the reverse current (see Fig. 6) have a smaller slope angle, $\tan\alpha \approx 1.8$, in comparison with their slope angle at the biases -0.3 V $< V < 0$ V, $\tan\alpha \approx 6.1$.

The slope of the ln I-V dependences is determined by the electric field strength E in the barrier through which the tunneling takes place [36]:

$$I = BN_t \exp\left(-4(2m^*)^{1/2}\varphi_{k1}^{1/2}/3q\hbar E\right). \quad (10)$$

The changes of the slope angle in the ln I-V dependences and the activation energy E_a at the reverse

voltage $V \sim -0.3$ V testify to the concentration of energy states in the forbidden gap at the n-Mn$_2$O$_3$/n-CdZnTe interface at the levels that are located by 0.3 eV below the equilibrium position of the Fermi level. According to the energy diagram, this is the location $E \approx E_V + 0.23$ eV with respect to the valence band top in n-CdZnTe.

The presence of acceptor levels at the depth $E_V + (0.2 \div 0.22)$ eV in the forbidden gap of cadmium telluride was established while carrying out theoretical calculations of the energy levels of intrinsic and impurity point defects in the framework of the *ab initio* method [37]. The authors of the cited work showed that the indicated energy levels correspond to the impurity atoms of the first group, which are arranged over the sites in the cadmium sublattice, namely, Cu$_{Cd}$, Au$_{Cd}$, and Ag$_{Cd}$. The arrangement of the energy levels $E_V + (0.2 \div 0.22)$ eV calculated on the basis of quantum-mechanical methods correlates well with experimental results [38, 39]. In particular, it was found that the presence of the energy level $E_V + 0.24$ eV in cadmium telluride crystals does not depend on the method of their growing, heat treatment conditions, and the nature of doping impurity [39]. This fact allowed the indicated level to be interpreted as the energy arrangement of the levels of an uncontrolled impurity. The most probable impurity is copper, the concentration of which in undoped CdTe amounts, as a rule, to 10^{16} cm^{-3}.

The C-V characteristics of the isotype n-Mn$_2$O$_3$/n-CdZnTe heterostructure were studied within the frequency interval of a measuring signal 10 kHz $< f <$ < 1000 kHz (Fig. 7). Due to the presence of an inversion layer near the heterocontact on the n-CdZnTe side and a high-impedance layer in the Mn$_2$O$_3$ film, a number of specific features take place, which are typical of MIS structures [31].

The dependence $C(V)$ is affected by the diffusion capacitance C_D of the contact region in the n-CdZnTe semiconductor and the capacitance C_F of the charge carrier depletion region in the film. The capacitances C_D and C_F are connected in series, and the total capacitance of the n-Mn$_2$O$_3$/n-CdZnTe heterostructure is determined by the relationship for the equivalent circuit (see the inset in Fig. 7, a)

$$\frac{1}{C} = \frac{1}{C_D} + \frac{1}{C_F}. \quad (11)$$

In the absence of external voltage ($V = 0$ V), there arises an inverse layer in the n-Mn$_2$O$_3$/n-CdZnTe heterostructure (Fig. 2) due to the combined action of the electron work function difference and the negative charge of the states in the n-CdZnTe semiconductor at the material interface (in the region contacting with Mn$_2$O$_3$). The total capacitance of the structure at the frequency $f = 10$ kHz and the voltage $V = 0$ V is equal to $C = 3.5$ nF (Fig. 7, *a*). At the non-zero reverse bias, this parameter slightly increases to 4 nF (at $V = -2$ V). The capacitance C_F at the non-zero reverse bias is determined by the thickness of the depletion region in the Mn$_2$O$_3$ film (the in-series connection of the barrier from the Mn$_2$O$_3$ side).

In the voltage interval -2 V $< V < 0$ V, the n-Mn$_2$O$_3$/n-CdZnTe heterostructure enters the strong inversion regime, which is responsible for a substantial growth of the capacitance C_D. In this case, the inequality $C_D \gg C_F$ is obeyed, and, according to Eq. (11), the total capacitance of the heterostructure $C \approx C_F$. The experimentally observed weak dependence of C_F on the reverse bias voltage is associated with the narrowing of the depletion region in Mn$_2$O$_3$. When changing to the strong inversion conditions (the band bending $q\varphi_{k2}(\text{inv}) \approx 2q\varphi_{k2}$), the thickness d_2 of the depletion region in n-CdZnTe saturates. Its maximum value W_m is determined by the formula [31]

$$W_m = \sqrt{\frac{4kT\varepsilon_0\varepsilon_S \ln\frac{N_{D2}}{n_i}}{N_{D2}q^2}},\qquad(12)$$

where $N_{D2} = n$ at $T = 300$ K, $n_i = 10^6$ cm^{-3} is the intrinsic concentration of charge carriers in CdZnTe, ε_S is the dielectric permittivity of the semiconductor (for CdZnTe, $\varepsilon_S = 10$ [28]), and $\varepsilon_0 =$ $= 8.85 \times 10^{-12}$ F/m.

Being calculated according to expression (12), the maximum thickness of the inversion layer in the n-CdZnTe contact region is equal to $W_m = 0.4$ μm. At reverse voltages across the n-Mn$_2$O$_3$/n-CdZnTe heterostructure, the charge density in the inversion layer increases, and the external electric field does not penetrate into it. The further broadening of the inverse region is so insignificant, that it weakly affects the capacitance C_D in the C-V plots in the voltage interval -2 V $< V < 0$ V (Fig. 7).

In the strong inversion regime, when the band bending in n-CdZnTe $q\varphi_{k2}(\text{inv}) \approx 2q\varphi_{k2} \approx 1.8$ eV,

the total capacitance of the structure with the thin depletion layer d_1 in n-Mn$_2$O$_3$ (Fig. 7, *b*) equals [31]

$$C_{min} = \frac{\varepsilon_0\varepsilon_{S1}}{d_1 + \frac{\varepsilon_{S1}}{\varepsilon_{S2}}W_m}.\qquad(13)$$

The determination of the $C_{\min}$-value from the experimental high-frequency ($f = 1000$ kHz) C-V characteristics (Fig. 7, *b*) allows the thickness d_1 of the depletion region in the n-Mn$_2$O$_3$ film to be estimated at the reverse biases $V_r \approx 1.8 \div 2$ V. Formula (13) gives the value $d_1 \approx 50$ nm. This result testifies that the reverse tunneling current in the n-Mn$_2$O$_3$/n-CdZnTe structure is realized via a multistage process that is possible only with the participation of states in the forbidden gap of n-Mn$_2$O$_3$, because the probability of forward tunneling into the n-CdZnTe states through a 0.3-eV barrier with the thickness $d_1 \approx 50$ nm is close to zero.

In the case of forward biases within the interval from zero to about 1 V across the n-Mn$_2$O$_3$/n-CdZnTe heterostructure, the region d_1 (depleted from the majority charge carriers) in the n-Mn$_2$O$_3$ film becomes wider, and its capacitance C_F decreases. The region d_2 on the n-CdZnTe side exits from the inversion regime, and its capacitance C_D increases due to a reduction of its thickness. The growth of C_D manifests itself in a frequency interval of 60–1000 kHz (Fig. 7, *b*). At forward voltages up to about 1 V, $C_D \gg C_F$, and, according to Eq. (11), the total capacitance $C \approx C_F$.

At $V > 1$ V, the thickness of the depletion region in the n-Mn$_2$O$_3$ film becomes equal to the film thickness, and the total capacitance C of the heterostructure does not depend on the applied voltage (Fig. 7). Being evaluated in the constant-capacitance section at $V > 1$ V according to the formula $w =$ $= \varepsilon_0\varepsilon_{S2}S/C$, where S is the heterojunction area, the Mn$_2$O$_3$ film thickness equals $w = 0.5$ μm. This value is also obtained, when studying the film within the multibeam interference method.

At the frequencies $f > 50$ kHz, the diffusion capacitance of the n-Mn$_2$O$_3$/n-CdZnTe structure, which corresponds to the inversion layer (at $V < 0$ V), decreases with the increasing frequency (Fig. 7, *b*). This occurs as a result of a reduction in the ability of charge carriers to follow the alternating signal. This ability is governed by the generation and recombination rates in the contact region of n-CdZnTe. For silicon-based structures, the minimum values of the
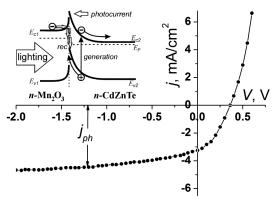
Fig. 8. *I-V* characteristic of the n-Mn$_2$O$_3$/ n-CdZnTe heterostructure under irradiation (AM1.5 (100 mW/cm^2) at $T =$ $= 295$ K. The mechanism of the photocurrent flow at $V < 0$ V is shown in the inset

capacitance C_{min} were observed at the frequencies $f \approx 100$ kHz [31]. For the researched n-Mn$_2$O$_3$/n-CdZnTe structures, it is possible to observe $C_{\min}$ at the frequency $f = 1000$ kHz, which is an order of magnitude higher. This fact points to a higher limiting frequency of the n-Mn$_2$O$_3$/n-CdZnTe heterostructures due to the high rate of generation-recombination processes in n-CdZnTe.

The *I-V* characteristics of the isotype n-Mn$_2$O$_3$/n-CdZnTe heterostructures irradiated from the n-Mn$_2$O$_3$ side under conditions close to AM1.5 (100 mW/cm^2) demonstrate the generation of the photocurrent $j_{ph} \approx 4$ mA/cm^2 at reverse biases larger than 1 V (Fig. 8). Under irradiation, the n-Mn$_2$O$_3$/n-CdZnTe heterostructure generates the photo-emf $V_{OC} = 0.36$ V in the open-circuit mode. The photocurrent density in the short-circuit mode $J_{SC} \approx$ ≈ 3.24 mA/cm^2. The main role in the photocurrent formation is played by the photogeneration process in n-CdZnTe (the inset in Fig. 8). The recombination processes of electrons from the n-Mn$_2$O$_3$ conduction band with photogenerated holes in n-CdZnTe also take part in the formation of the photocurrent flow.

4. Conclusions

Isotype n-Mn$_2$O$_3$/n-CdZnTe heterostructures with a current rectification coefficient of about 10^4 were fabricated using the spray pyrolysis of a 0.1 M aqueous solution of MnCl$_2 \cdot 4$H$_2$O salt on the surface of crystalline n-CdZnTe substrates heated to $T_S =$ $= 350$ °C. The diode characteristics of the hetero-

junction are governed by an energy barrier 0.9 eV in height, which arises on the n-CdZnTe side. The barrier is formed by a combined action of the energy states located at the interface between the n-Mn$_2$O$_3$ and n-CdZnTe semiconductors and the difference between the work functions of those semiconductors.

In the forward-voltage interval $3kT/q < V < 0.9$ V, the current flows through the n-Mn$_2$O$_3$/n-CdZnTe heterostructure owing to the tunneling of electrons from the states in the n-CdZnTe conduction band into the n-Mn$_2$O$_3$ conduction band through the barrier. The analysis of the forward-current tunneling mechanism made it possible to reveal a depletion of electrically active impurities in the n-CdZnTe contact region owing to the evaporation of cadmium atoms from the n-CdZnTe near-surface region, when the substrates were heated in the course of spray pyrolysis.

The reverse current at the bias voltages -2 V $<$ $< V < -3kT/q$ is formed by the multistage tunneling of electrons from the bottom of the n-Mn$_2$O$_3$ conduction band to the states in the forbidden gap in the heterojunction space-charge region and their further recombination with holes in the valence band of the inverse layer in n-CdZnTe. According to the analysis of how the tunneling activation energy changes with the reverse bias, the location of the energy states arising at the heterojunction interface and contributing to the formation of the potential barrier height was established to equal $E \approx E_V(\text{CdZnTe}) + 0.23$ eV.

The *C-V* characteristics of the n-Mn$_2$O$_3$/n-CdZnTe heterostructure are formed by the combined action of the diffusion capacitance of the inverse layer in n-CdZnTe and the capacitance of the n-Mn$_2$O$_3$ film. The capacitance minimum for the n-Mn$_2$O$_3$/n-CdZnTe structure in the inversion mode is observed at a frequency of about 1 MHz, which is an order of magnitude higher than the corresponding parameter for silicon-based MIS structures. This fact testifies to high values of the limiting frequency for the studied heterostructure and is favorable for the application of the latter in high-speed photoelectric devices.

1. S.V. Ovsyannikov, A.M. Abakumov, A.A. Tsirlin, W. Schnelle, R. Egoavil, J. Verbeeck, G. Van Tendeloo, K.V. Glazyrin, M. Hanfland, L. Dubrovinsky. Perovskite-like Mn$_2$O$_3$: A path to new manganites. *Angew. Chem. Int. Ed.* **52**, 1494 (2013).

2. F. Hong, B. Yue, N. Hirao, Z. Liu, B. Chen. Significant improvement in Mn_2O_3 transition metal oxide electrical conductivity via high pressure. *Sci. Rep.* **7**, 44078 (2017).

3. M. Wang, M. Shen, L. Zhang, J. Tian, X. Jin, Y. Zhou, J. Shi. 2D-2D MnO_2/g-C_3N_4 heterojunction photocatalyst: In-situ synthesis and enhanced CO_2 reduction activity. *Carbon* **120**, 23 (2017).

4. T. Yu, Y. Sun, C. Zhe, W. Wang, P. Rao. Synthesis of synthesis of CuO_x/MnO_2 heterostructures with enhanced visible light-driven photocatalytic activity. *J. Mater. Sci. Chem. Eng.* **5**, 12 (2017).

5. W. Ren, D. Liu, C. Sun, X. Yao, J. Tan, C. Wang, K. Zhao, X. Wang, Q. Li, L. Mai. Nonhierarchical heterostructured Fe_2O_3/Mn_2O_3 porous hollow spheres for enhanced lithium storage. *Small* **14**, 1800659 (2018).

6. S. Sharma, P. Chauhan, S. Husain. Structural and optical properties of Mn_2O_3 nanoparticles and its gas sensing applications. *Adv. Mater. Proc.* **1**, 220 (2016).

7. R. Naeem, M. Ali Ehsan, R. Yahya, M. Sohail, H. Khaledi, M. Mazhar. Fabrication of pristine Mn_2O_3 and Ag–Mn_2O_3 composite thin films by AACVD for photoelectrochemical water splitting. *Dalton Trans.* **45**, 14928 (2016).

8. H.D. Awad, A.K. Elttayef, A.L. Ressen, K.A. Ali. The effect of annealing on the structural and optical properties of Mn_2O_3 thin film prepared by chemical spray pyrolysis. *Int. J. Sci. Res.* **6**, 291 (2017).

9. A.L. Fahrenbruch, R.H. Bube. *Fundamentals of Solar Cells* (Academic Press, 1983) [ISBN: 9780323145381].

10. A. Ginsburg, D.A. Keller, H.-N. Barad, K. Rietwyk, Y. Bouhadana, A. Anderson, A. Zaban. One-step synthesis of crystalline Mn_2O_3 thin film by ultrasonic spray pyrolysis. *Thin Solid Films* **615**, 261 (2016).

11. Q. Javed, W. Feng-Ping, M.Y. Rafique, A.M. Toufiq, M.Z. Iqbal. Canted antiferromagnetic and optical properties of nanostructures of Mn_2O_3 prepared by hydrothermal synthesis. *Chin. Phys. B* **21**, 117311 (2012).

12. M. Chandra, S. Yadav, S. Rayaprol, K. Singh. Structural and impedance spectroscopy of α-Mn_2O_3. *AIP Conf. Proc.* **1942**, 110023 (2018).

13. A. Ramirez, P. Hillebrand, D. Stellmach, M.M. May, P. Bogdanoff, S. Fiechter. Evaluation of MnO_x, Mn_2O_3, and Mn_3O_4 electrodeposited films for the oxygen evolution reaction of water. *J. Phys. Chem. C* **118**, 14073 (2014).

14. S. Pishdadian, A.M. Shariati Ghaleno. Influences of annealing temperature on the optical and structural properties of manganese oxide thin film by Zn doping from sol-gel technique. *Acta Phys. Pol. A* **123**, 471 (2013).

15. I.P. Koziarskyi, E.V. Maistruk, I.G. Orletsky, M.I. Ilashchuk, D.P. Koziarskyi, P.D. Marianchuk, M.M. Solovan, K.S. Ulyanytsky. Influence of properties of thin films on electrical characteristics of isotype heterojunctions Fe_2O_3/n-CdTe. *Semicond. Sci. Technol.* **35**, 025018 (2020).

16. V.V. Khomyak, V.V. Brus, M.I. Ilashchuk, I.G. Orletsky, I.I. Shtepliuk, G.V. Lashkarev. Fabrication and properties of the photosensitive anisotype n-$Cd_xZn_{1-x}O/p$-CdTe heterojunctions. *Acta Phys. Pol. A* **126**, 1163 (2014.

17. I.G. Orletskyi, M.I. Ilashchuk, M.M. Solovan, P.D. Maryanchuk, E.V. Maistruk, G.O. Andrushchak. Effect of fabrication conditions on charge transport and photo-response of n-ITO/p-$Cd_{1-x}Zn_x$Te heterojunctions. *Mater. Res. Express* **6**, 086219 (2019).

18. E.V. Maistruk, I.G. Orletsky, M.I. Ilashchuk, I.P. Koziarskyi, D.P. Koziarskyi, P.D. Marianchuk, O.A. Parfenyuk. Influence of heat treatment of the base material on the electrical properties of anisotyped heterojunctions n-ZnO : Al/p-CdZnTe. *Semicond. Sci. Technol.* **34**, 045016 (2019).

19. J.J. Kennedy, P.M. Amirtharaj, P.R. Boyd, S.B. Qadri, R.C. Dobbyn, G.G. Long. Growth and characterization of $Cd_{1-x}Zn_x$Te and $Hg_{1-y}Zn_y$Te. *J. Cryst. Growth* **86**, 93 (1988).

20. K. Guergouri, R. Triboulet, A. Tromson-Carli, Y. Marfaing. Solution hardening and dislocation density reduction in CdTe crystals by Zn addition. *J. Cryst. Growth* **86**, 61 (1988).

21. A. Ramirez, D. Friedrich, M. Kunst, S. Fiechter. Charge carrier kinetics in MnO_x, Mn_2O_3 and Mn_3O_4 films for water oxidation. *Chem. Phys. Lett.* **568–569**, 157 (2013).

22. L. Jayaselvan, C.G. Sambandam, C. Ravidhas, A.M.E. Raj. Effect of preparative parameters on structural, optical and electrical properties of Mn_2O_3 nanoparticles prepared via microwave assisted technique. *Int. J. Sci. Res. Sci. Technol.* **3**, 106 (2017).

23. I.G. Orletskii, P.D. Mar'yanchuk, E.V. Maistruk, M.N. Solovan, V.V. Brus. Low-temperature spray pyrolysis of FeS_2 films and their electrical and optical properties. *Phys. Solid State* **58**, 37 (2016).

24. I.G. Orletskyi, M.I. Ilashchuk, E.V. Maistruk, M.M. Solovan, P.D. Maryanchuk, S.V. Nichyi. Electrical properties of SIS heterostructures n-$SnS_2/CdTeO_3/p$-CdZnTe. *Ukr. J. Phys.* **64**, 164 (2019).

25. I.G. Orletskyi, M.I. Ilashchuk, M.N. Solovan, P.D. Maryanchuk, O.A. Parfenyuk, E.V. Maistruk, S.V. Nichyi. Electrical properties and energy parameters of n-FeS_2/p-$Cd_{1-x}Zn_x$Te heterojunctions. *Semiconductors* **52**, 1171 (2018).

26. Y. Xi, T. Gessmann, J. Xi, J.K. Kim, J.M. Shah, E.F. Schubert, A.J. Fischer, M.H. Crawford, K.H. Bogart, A.A. Allerman. Junction temperature in ultraviolet light-emitting diodes. *Jpn. J. Appl. Phys* **44**, 7260 (2005).

27. J.P. Ponpon. A review of ohmic and rectifying contacts on cadmium telluride. *Solid-State Electron.* **28**, 689 (1985).

28. A. Luque, S. Hegedus. *Handbook of Photovoltaic Science and Engineering* (Wiley, 2011) [ISBN: 978-0-470-72169-8].

29. J.J. Prias-Barragan, L. Tirado-Mejia, H. Ariza-Calderon, L. Banos, J.J. Perez-Bueno, M.E. Rodriguez. Band gap energy determination by photoacoustic absorption and optical analysis of $Cd_{1-x}Zn_x$Te for low zinc concentrations. *J. Cryst. Growth* **286**, 179 (2006).

30. J. Franc, P. Hlidek, P. Moravec, E. Belas, P. Hoschl, L. Turjanska, R. Varghova. Determination of energy gap in $Cd_{1-x}Zn_xTe$ ($x = 0$–0.06). *Semicond. Sci. Technol.* **15**, 561 (2000).

31. S.M. Sze, K.N. Kwok. *Physics of Semiconductor Devices* (Wiley, 2006) [ISBN: 9780471143239].

32. S. Lany. Semiconducting transition metal oxides. *J. Phys.: Condens. Matter.* **27**, 283203 (2015).

33. B.L. Sharma, R.K. Purohit. *Semiconductor Heterojunctions* (Pergamon Press, 1974) [ISBN: 9781483280868].

34. M. Chandra, S. Yadav, R.J. Choudhary, R. Rawat, A.K. Sinha, M.-B. Lepetit, K. Singh. Multiferroicity and magnetoelastic coupling in α-Mn_2O_3: A binary perovskite. *Phys. Rev. B* **98**, 104427 (2018).

35. E. Maistruk, M. Ilashchuk, I. Orletskyi, I. Koziarskyi, D. Koziarskyi, P. Maryanchuk, O. Parfenyuk, K. Ulyanytsky. Influence of the base material on the interface properties of $ZnO:Al/n$-CdS/p-$Cd_{1-x}Zn_xTe$ heterojunctions. *Eng. Res. Express* **2**, 035037 (2020).

36. A.G. Milnes, D.L. Feucht. *Heterojunctions and Metal-Semiconductor Junctions* (Academic Press, 1972) [ISBN: 0124980503].

37. S.-H. Wei, S.B. Zhang. Chemical trends of defect formation and doping limit in II-VI semiconductors: The case of CdTe. *Phys. Rev. B* **66**, 155211 (2002).

38. A.V. Savitsky, M.I. Ilashchuk, O.A. Parfenyuk, K.S. Ulyanytsky, V.R. Burachek, R. Ciach, Z. Swiatek, Z. Kuznicki. Thermostability of physical properties of cadmium telluride crystals. *Thin Solid Films* **361**−**362**, 203 (2000).

39. K. Yokota, S. Katayama, T. Yoshikawa. Termally-stimulated current in p-type CdTe annealed in various atmospheres. *Jpn. J. Appl. Phys.* **21**, 456) (1982).

40. F.T.J. Smith. Electrically active point defects in cadmium telluride. *J. Metallurg. Trans.* **1**, 617 (1970).

І.Г. Орлецький, М.І. Ілащук,
Е.В. Майструк, Г.П. Пархоменко, П.Д. Мар'янчук

ЕЛЕКТРИЧНІ ВЛАСТИВОСТІ
І ЕНЕРГЕТИЧНІ ПАРАМЕТРИ ФОТОЧУТЛИВИХ
ГЕТЕРОСТРУКТУР n-Mn_2O_3/n-CdZnTe

Досліджено умови виготовлення фотодіодних ізотипних гетероструктур n-Mn_2O_3/n-CdZnTe методом спрей-піролізу тонких плівок біксбіту α-Mn_2O_3 на кристалічні підкладинки n-CdZnTe. За температурними залежностями I-V-характеристик проаналізовано механізми тунелювання електронів крізь енергетичний бар'єр гетеропереходу при прямому та зворотному струмах. З'ясована роль енергетичних станів на межі n-Mn_2O_3/n-CdZnTe у формуванні параметрів бар'єра. На основі C-V-характеристик встановлено динаміку зміни і взаємозв'язок ємнісних параметрів тонкої плівки n-Mn_2O_3 та інверсійного шару n-CdZnTe. Представлено модель енергетичної діаграми гетеропереходу n-Mn_2O_3/n-CdZnTe. Проаналізовано фотоелектричні властивості гетероструктури.

Ключові слова: тонка плівка, спрей-піроліз, гетероструктура, енергетична діаграма, фотодіод.